Dynein efficiently navigates the dendritic cytoskeleton to drive the retrograde trafficking of BDNF/TrkB signaling endosomes

Swathi Ayloo[a,b,†], Pedro Guedes-Dias[b], Amy E. Ghiretti[b], and Erika L. F. Holzbaur[b,*]
[a]Department of Biology, School of Arts and Sciences, and [b]Department of Physiology and the Pennsylvania Muscle Institute, Perelman School of Medicine, University of Pennsylvania, Philadelphia, PA 19104

ABSTRACT The efficient transport of cargoes within axons and dendrites is critical for neuronal function. Although we have a basic understanding of axonal transport, much less is known about transport in dendrites. We used an optogenetic approach to recruit motor proteins to cargo in real time within axons or dendrites in hippocampal neurons. Kinesin-1, a robust axonal motor, moves cargo less efficiently in dendrites. In contrast, cytoplasmic dynein efficiently navigates both axons and dendrites; in both compartments, dynamic microtubule plus ends enhance dynein-dependent transport. To test the predictions of the optogenetic assay, we examined the contribution of dynein to the motility of an endogenous dendritic cargo and found that dynein inhibition eliminates the retrograde bias of BDNF/TrkB trafficking. However, inhibition of microtubule dynamics has no effect on BDNF/TrkB motility, suggesting that dendritic kinesin motors may cooperate with dynein to drive the transport of signaling endosomes into the soma. Collectively our data highlight compartment-specific differences in kinesin activity that likely reflect specialized tuning for localized cytoskeletal determinants, whereas dynein activity is less compartment specific but is more responsive to changes in microtubule dynamics.

INTRODUCTION

The transport of organelles within the axonal and dendritic compartments of neurons is fundamental to the development and function of these highly polarized cells. Long-range transport of cargoes including mitochondria, endosomes, and vesicles is primarily mediated by dynein and kinesin motors moving along the microtubule cytoskeleton (Maday *et al.*, 2014). The differing organization of the microtubule cytoskeleton within axons and dendrites of mammalian neurons provides an important mechanism to ensure compartment-specific trafficking. Microtubules within axons form a unipolar plus-end out, tiled array (Baas *et al.*, 1988; Kleele *et al.*, 2014; Yogev *et al.*, 2016), such that plus-end–directed kinesins drive anterograde trafficking and minus-end–directed dynein drives retrograde trafficking along the axon. In contrast, microtubules in the dendrites of mammalian neurons are oriented with mixed polarity (Baas *et al.*, 1988; Kleele *et al.*, 2014). As a consequence, much less is known about the differential function of kinesin and dynein motors in cargo transport in dendrites.

Many studies have been directed toward understanding the polarized sorting of kinesins from the soma *to* axons or dendrites (Setou *et al.*, 2002; Nakata and Hirokawa, 2003; Jacobson *et al.*, 2006; Song *et al.*, 2009; Huang and Banker, 2012; van Spronsen *et al.*, 2013). Collectively this work suggests a multilayered regulation of selective kinesin transport. Recent studies have begun to identify kinesins that are effective motors *within* dendrites (Jenkins *et al.*, 2012; Farkhondeh *et al.*, 2015; Ghiretti *et al.*, 2016; Muhia *et al.*, 2016), but the mechanisms allowing some, but not all, kinesins

Abbreviations used: ANOVA, one-way analysis of variance; BDNF, brain-derived neurotrophic factor; BICD, bicaudal D2; CLIP-170, cytoplasmic linker protein CLIP-170; cTMP, photocaged trimethoprim; DIV, days in vitro; DMSO, dimethyl sulfoxide; EB1/3, microtubule end-binding protein 1/3; eDFHR, *Escherichia coli* dihydrofolate reductase; GFP, green fluorescent protein; GRIP1, glutamate receptor-interacting protein 1; K560, 1–560 aa kinesin-1 heavy chain; KIF, kinesin family; Noco, nocodazole; Qdots, quantum dots; RFP, red fluorescent protein; STED, stimulated emission depletion; TrkB, tyrosine receptor kinase B.

to function effectively in this compartment are not yet understood. Similarly, dynein is a well-characterized axonal motor (Maday *et al.*, 2014), and has been shown to drive cargo from the soma *into* dendrites (Kapitein *et al.*, 2010). However, comparatively little is known about the ability of dynein to effectively drive trafficking *within* dendrites.

Given the mixed polarity of the dendritic microtubule cytoskeleton, it is not yet clear how a unidirectional motor like dynein or kinesin could effectively move cargo within this compartment. Recent models propose that the net motility of a given cargo is likely determined by the combined activities of multiple types of motor proteins that differentially regulate distinct aspects of transport (Arpag *et al.*, 2014; Prevo *et al.*, 2015; Ruane *et al.*, 2016). This multiple motor hypothesis is particularly intriguing when it comes to dendritic transport, as both dynein and kinesins could mediate the trafficking of a given cargo in the same direction. The relative contribution of multiple motors to the trafficking of a given cargo, and the mechanisms that might differentially regulate the activities of these motors, can be difficult to determine from the analysis of endogenous cargo motility alone. Thus new techniques that allow for assessment of the relative effectiveness of a single motor type within the complex dendritic cytoskeleton are of critical importance to develop a full understanding of neuronal transport.

In this study, we applied a novel optogenetic tool (Ballister *et al.*, 2014, 2015) to recruit dynein and kinesin motors to specific organelles within axons or dendrites, and examined the effects on organelle dynamics immediately post recruitment. We demonstrate that kinesin-1 functions much more effectively in axons than dendrites, while, surprisingly, dynein is just as efficient a motor in either compartment. Further, we find that dynein motility is modulated by microtubule dynamics in both axons and dendrites. In conjunction with recent work showing enhanced recruitment of dynein to microtubules enriched in tyrosinated tubulin in axons (Nirschl *et al.*, 2016), these observations suggest that posttranslational modifications of the microtubule cytoskeleton, and in particular the tyrosination state of the tubulin tail, also regulate dynein activity in dendrites. Finally, we test the predictions of our optogenetic assay by analyzing the contribution of dynein motors to the trafficking of an endogenous cargo, BDNF/TrkB-positive signaling endosomes, and find that dynein is required to establish the retrograde bias of BDNF/TrkB motility seen in dendrites. Together these studies provide further insight into the mechanisms regulating the compartment-specific transport of organelles within neurons.

RESULTS

Recruitment of dynein or kinesin to peroxisomes in dendrites induces robust bidirectional motility

To selectively recruit motor proteins to organelles with high spatial and temporal resolution, we used a recently developed light-inducible dimerization tool (Ballister *et al.*, 2014). Briefly, in this system, two proteins of interest are tagged with Halo and eDHFR, respectively. The addition of the caged, membrane-permeable dimerizer cTMP-HaloLigand allows for the dimerization of the tagged proteins following localized activation with a 405 nm laser (Figure 1A). In contrast to rapalog, an analogue of rapamycin used to chemically induce dimerization in the whole cell (Kapitein *et al.*, 2010; Jenkins *et al.*, 2012; Bentley *et al.*, 2015), our light-inducible dimerization system enables the localized recruitment of motor proteins to specific organelles (Figure 1A). The ability to spatially control motor recruitment allows us to examine compartment-specific and organelle-dependent regulation of motility. With this system, we can

directly visualize motor recruitment and follow the subsequent changes in organelle dynamics in real time.

To assess kinesin-1–driven motility, we used a constitutively active form of the kinesin-1 motor, K560, which includes the first 560 residues of the kinesin heavy chain encoding both the N-terminal motor domain and coiled-coil sequences required for dimerization. For dynein recruitment, we used an N-terminal fragment of the adaptor protein Bicaudal D2, which effectively recruits dynein and its activator dynactin (Splinter *et al.*, 2012). We examined the recruitment of motors to peroxisomes, as these are mostly stationary organelles with low baseline motility (~20%; Ballister *et al.*, 2015) that are enriched in the soma and dendrites of neurons (Kapitein *et al.*, 2010).

In axons, recruitment of either kinesin-1 or dynein motors to peroxisomes induced unidirectional anterograde or retrograde motion, respectively (Figure 1B), as previously reported (Ballister *et al.*, 2015). Robust motility was observed in greater than 90% of axonal peroxisomes that were photoactivated (Ballister *et al.*, 2015). In contrast to the unidirectional motility observed in axons, recruitment of either K560 or BICD to dendritic peroxisomes induced long, bidirectional runs as shown in Figure 1C.

Dual-color imaging enabled us to visualize the specific recruitment of motor proteins or motor adaptors to the photoactivated organelles by an increase in the intensity of mCherry fluorescence, as indicated by arrowheads in the time series (Figure 1C). In the corresponding kymographs, peroxisomes that were initially green-only became yellow postphotoactivation, showing the comigration of organelles with the recruited K560 (left) or BICD (right). This induced recruitment of motors to peroxisomes within dendrites is best seen in stills of peroxisomes pre- and postphotoactivation (Figure 1D). Quantitation of the intensity change in mCherry fluorescence pre- and postphotoactivation revealed a (1.6 ± 0.7)-fold increase in the mCherry signal following K560 recruitment to peroxisomes in axons, and a (4.2 ± 0.4)-fold increase in mCherry fluorescence following K560 recruitment to peroxisomes in dendrites. Recruitment of BICD to axonal peroxisomes led to a (4.1 ± 0.6)-fold increase in fluorescence, whereas recruitment in dendrites led to a (6.0 ± 1.2)-fold increase in the intensity of mCherry (mean ± SEM; $n = 10$–12 neurons from two experiments in axons and three experiments in dendrites). Thus successful recruitment of K560 and BICD to peroxisomes was observed in both compartments. Of note, instances in which no motility of photoactivated organelles was observed following motor recruitment were not due to a lack of motor recruitment. This is shown in a representative example of a photoactivated peroxisome that displayed no motility despite a clear increase in the fluorescence intensity of mCherry, indicating successful K560 recruitment (Figure 1D).

Dynein-driven motility in dendrites has a retrograde bias

We observed a striking difference in the ability of kinesin or dynein recruitment to induce peroxisome motility within the dendritic compartment. Although recruitment of dynein induced motility in >90% of the photoactivated organelles, recruitment of K560 induced motility in only ~60% of photoactivated organelles (Figure 2A). This is in contrast to our observations in axons, where both K560 and dynein induced motility in >90% of photoactivated organelles (Figure 1B; Ballister *et al.*, 2015). Thus, targeted recruitment of dynein to peroxisomes induces movement as effectively in dendrites as axons, while kinesin-1 functions as a robust axonal motor but does not perform as efficiently in dendrites.

Examining the motor-induced movement of peroxisomes more closely, we found that photoactivated peroxisomes moved at a speed of 0.49 ± 0.03 μm/s (mean ± SEM), with no significant
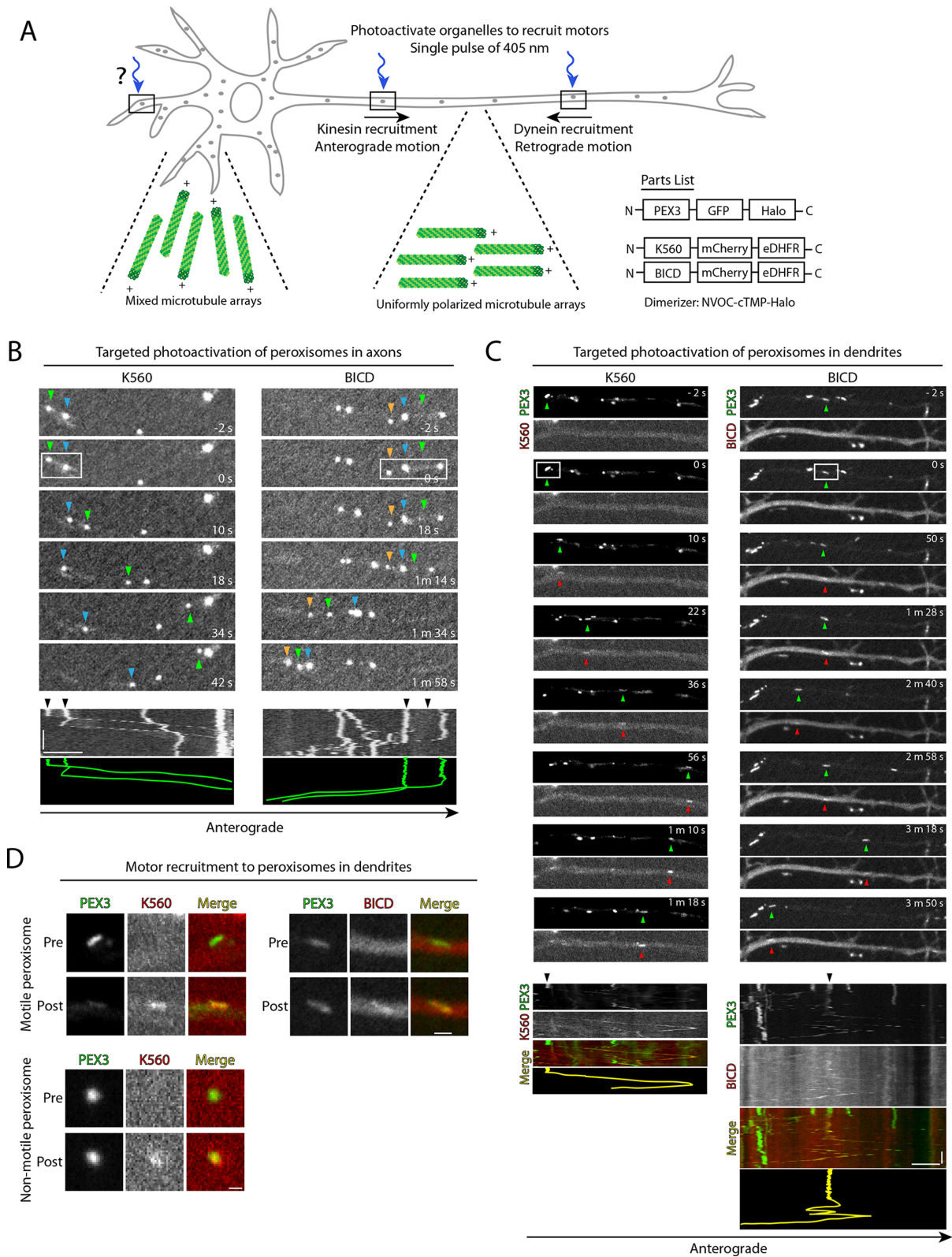
FIGURE 1: Recruitment of dynein or kinesin to peroxisomes in axons and dendrites. (A) Schematic and parts list of the light-inducible dimerization system implemented in mature neurons that have uniformly polarized microtubule arrays in the axon and mixed arrays in dendrites. (B) Time series and corresponding kymographs showing the anterograde movement of locally photoactivated peroxisomes (white box) in axons. Horizontal bar, 5 μm. Vertical bar, 1 min. (C) Time series and corresponding kymographs showing the bidirectional movement of locally photoactivated peroxisomes (white box) in dendrites. Horizontal bar, 5 μm. Vertical bar, 1 min. (D) Top panel, images of motor recruitment to peroxisomes pre- and postphotoactivation. Horizontal bar, 1 μm. Bottom panel, representative stills showing recruitment of K560 even in the case of peroxisomes that are immotile postphotoactivation. Horizontal bar, 500 nm.
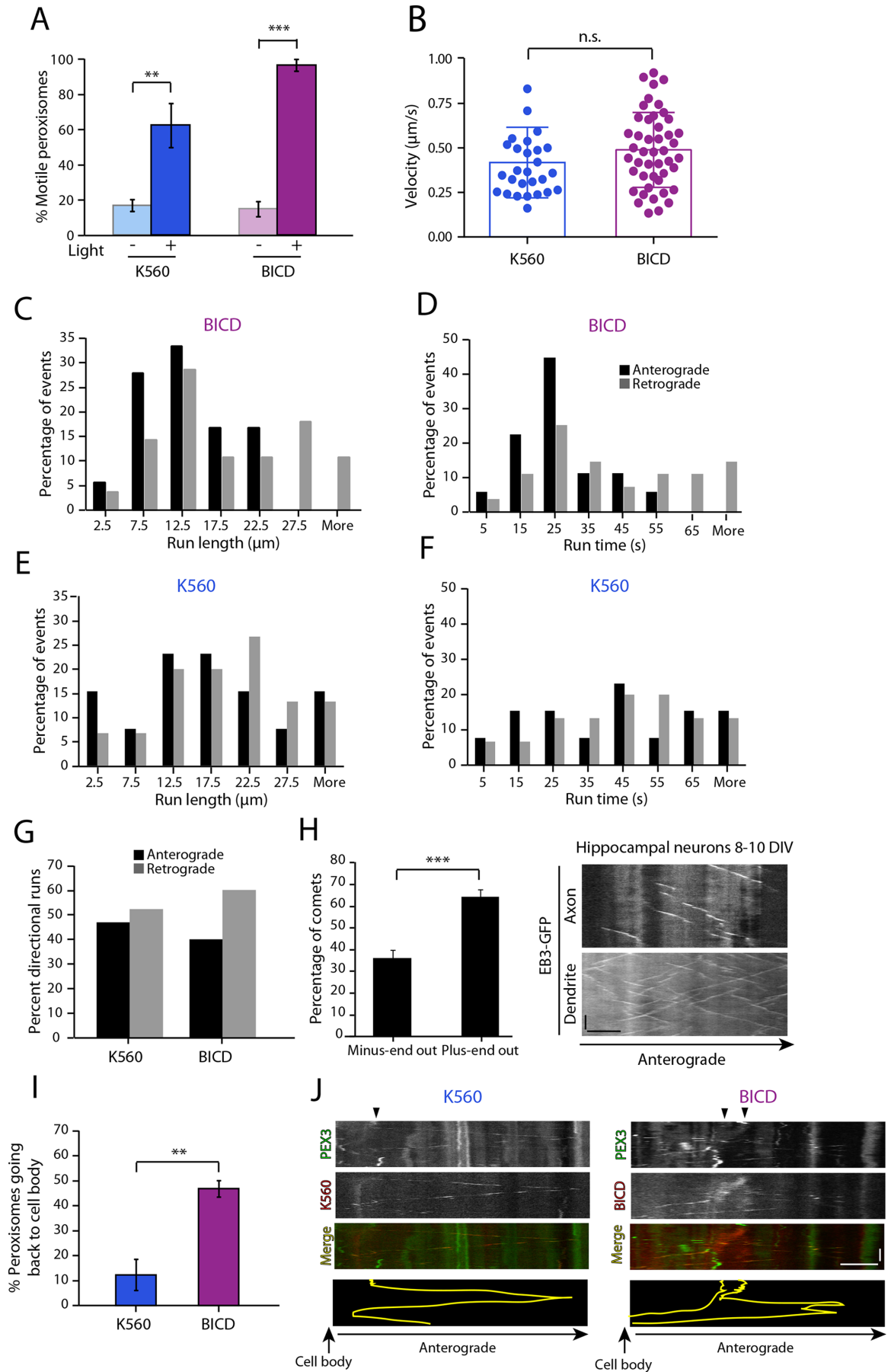
differences in the velocities induced by either kinesin or dynein recruitment (Figure 2B). We then measured the run lengths of motile organelles and found that dynein recruitment caused organelles to take more frequent and longer retrograde runs, indicative of a significant retrograde bias (Figure 2C). Similar to the observed run lengths, the run times of dynein-induced motion also exhibited a retrograde bias (Figure 2D). In contrast, K560 did not show any significant directional bias when recruited to organelles in dendrites (Figure 2, E and F).

To further explore the apparent retrograde bias in dynein motility in dendrites, we compared the percentage of runs in each direction for motile K560 and dynein events. We found that although K560-driven motility was equally divided between antero-grade- and retrograde-directed runs (47% anterograde vs. 53% retrograde; Figure 2G), dynein-driven motility showed a stronger bias for retrograde-directed runs (40% anterograde vs. 60% retrograde; Figure 2G). We compared this retrograde bias in dynein-driven motility to the overall organization of microtubules in hippocampal neurons under our culture conditions by assessing the directionality of EB3-GFP comets (Figure 2H). In proximal dendrites, $64 \pm 3.6\%$ of microtubules were plus-end out and $36 \pm 3.6\%$ were minus-end out (Figure 2H), consistent with previous reports (Baas et al., 1988; Stepanova et al., 2003; Kleele et al., 2014) and closely resembling the bias in dynein-driven motility (Figure 2G). Importantly, this organization was not altered by over-expression of the BICD or K560 constructs used in our assay (BICD: 65.18 ± 2.63; K560: 69.11 ± 2.16; mean plus-end out $\pm$ SEM; $n = 10$ neurons from two experiments). Thus the retrograde bias in dynein motility directly mirrors the underlying microtubule organization in dendrites.

The overall retrograde bias in dynein motility led to a pronounced difference in the eventual fates of motile organelles following recruitment of dynein or kinesin-1. Following recruitment of dynein to dendritic peroxisomes, ~50% of motile organelles underwent robust retrograde transport, eventually entering the cell soma (Figure 2, I and J). Once they entered the soma, these organelles did not reenter the dendrite during our imaging timeframe. In contrast, the productive relocation of organelles from dendrite to soma was only rarely (~10%) observed following kinesin-1 recruitment, even when we focused specifically on the motile population of vesicles (Figure 2, I and J). Together these findings demonstrate that dynein can effectively navigate the mixed polarity cytoskeleton found in dendrites, moving with a retrograde bias consistent with the underlying microtubule polarity. The relatively subtle retrograde bias in directionality, coupled with a retrograde bias in run length and time, is sufficient to effectively drive trafficking of cargo from dendrites to soma.

Dynein requires dynamic microtubules for efficient transport in both axons and dendrites

Recent work has shown that within axons, dynein is efficiently recruited to dynamic microtubule plus ends, through an interaction with dynactin, CLIP-170, and EB1 (Moughamian and Holzbaur, 2012; Moughamian et al., 2013; Nirschl et al., 2016). This mechanism is essential for efficient initiation of transport from the distal axon, and is disrupted in neurons expressing a point mutation in the dynactin subunit p150[Glued] that is causative for Perry Syndrome, a lethal form of Parkinsonism (Lloyd et al., 2012; Moughamian and Holzbaur, 2012). Contributing to this mechanism is an enhanced interaction of dynactin with tyrosinated microtubules that promotes the initiation of dynein-driven runs in vitro (McKenney et al., 2016; Nirschl et al., 2016). In neurons, tyrosinated tubulin is enriched in the dynamic microtubule population found at the axon terminal (Nirschl et al., 2016).

We wondered whether this mechanism might regulate dynein motility more broadly within the neuron. As a first step, we visualized the levels of tyrosinated/detyrosinated tubulin throughout the neuron using stimulated emission depletion (STED) and confocal microscopy. Then we treated neurons with either dimethyl sulfoxide (DMSO) or low-dose nocodazole (100 ng/ml, or 330 nM) to dampen microtubule dynamics. We observed a significant decrease in the levels of tyrosinated tubulin (Figure 3, A–C), accompanied by a significant increase in the levels of detyrosinated tubulin (Figure 3, D–F) in both axons and dendrites of nocodazole-treated neurons. Importantly, quantitation of β-tubulin staining did not reveal a loss of overall microtubule polymer in neurons treated with low-dose nocodazole as compared with DMSO-treated control neurons (Figure 3, G and H), indicating that at this concentration the drug is effectively dampening microtubule dynamics without inducing microtubule depolymerization.

Next we asked whether the dynein-induced motility of peroxisomes in neurons would show a dependence on the presence of dynamic microtubule plus ends. To test this possibility, we performed our photoactivation assay recruiting either kinesin-1 or dynein to peroxisomes in neurons treated with low-dose nocodazole for 1.5 h before imaging; under these conditions, microtubule dynamics were eliminated, as shown in the EB3 kymographs from axons and dendrites (Figure 4A).

We first examined the effects of dampening microtubule dynamics on the kinesin and dynein-driven motility of photoactivated peroxisomes in axons. Low-dose nocodazole treatment had no effect on K560-driven motility in axons (Figure 4, B and C). Recruitment of kinesin induced robust anterograde motion of peroxisomes similar to that observed in control experiments, shown in the kymographs in Figure 4B. In contrast, we observed a significant reduction in the dynein-induced motility of peroxisomes in axons treated with

---

FIGURE 2: Kinesin-1 moves inefficiently while dynein has a retrograde bias in dendrites. (A) Percentage of photoactivated peroxisomes that are motile in dendrites. Mean ± SEM, **$p < 0.01$, ***$p < 0.001$, Student's t test. (B) Average velocity of motile photoactivated peroxisomes following dynein or K560 recruitment. Mean ± SEM, n.s. = not significant, Student's t test. (C–F) Histograms of run length and run time of the individual runs of motile peroxisomes following recruitment of dynein (C, D) or K560 (E, F). (G) Quantitation of the overall percent of peroxisome runs in the anterograde vs. retrograde direction upon motor recruitment. Data from 25 peroxisomes from $n = 12$ neurons and $N = 3$ independent experiments. (H) Quantitation of directionality of EB3 comets in dendrites and representative kymographs in the axon and dendrites of mature hippocampal neurons, 8–10 DIV. Mean ± SEM, $n = 10$ neurons from $N = 2$ independent experiments. Horizontal bar, 5 μm. Vertical bar, 30 s. (I) Quantitation of percent of peroxisomes going back to the cell body postphotoactivation. Mean ± SEM, **$p < 0.01$, Student's t test. Data from 25 peroxisomes from $n = 12$ neurons and $N = 3$ independent experiments. (J) Representative examples showing bidirectional movement of peroxisomes upon K560 recruitment or going back to the cell body upon dynein recruitment. Horizontal bar, 5 μm. Vertical bar, 1 min.
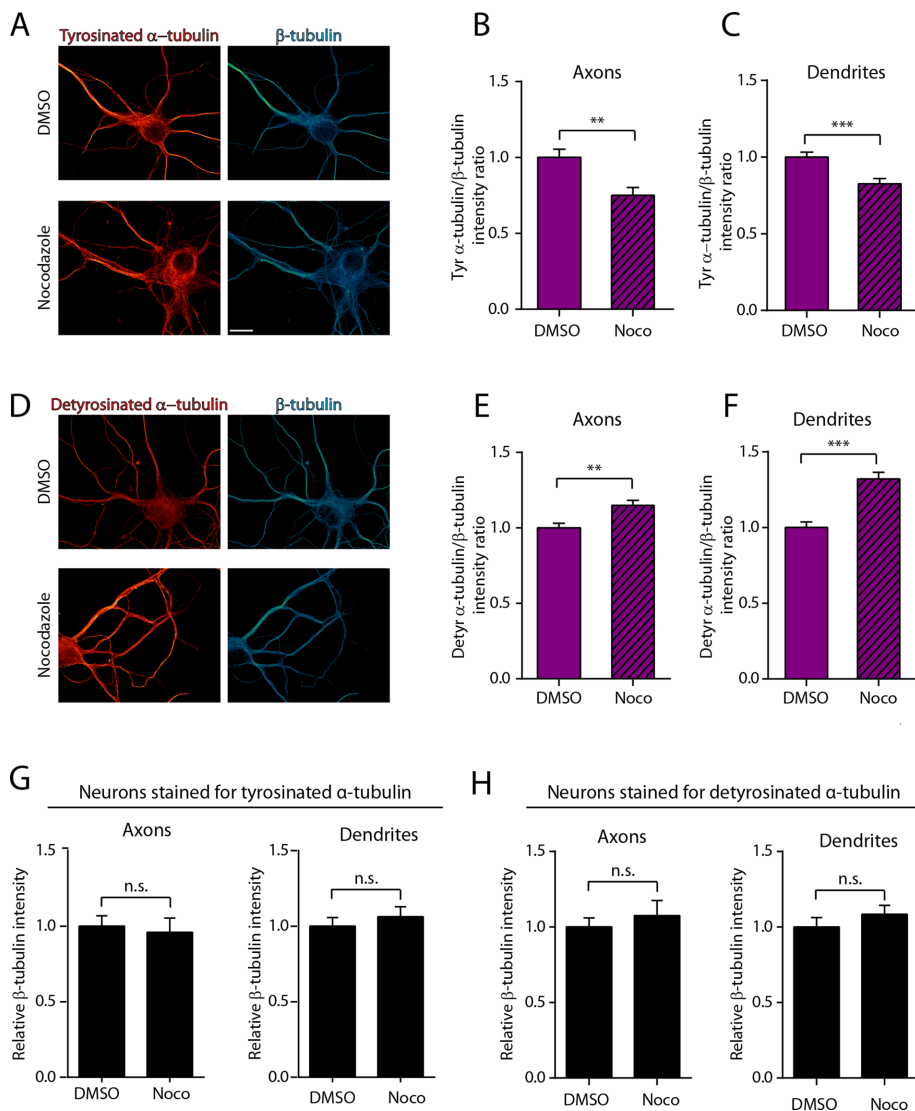
FIGURE 3: Low-dose nocodazole treatment decreases tubulin tyrosination. (A) Representative deconvolved maximum projections of STED images of tyrosinated tubulin in hippocampal neurons with and without low-dose nocodazole treatment. (B) Axonal and (C) dendritic quantification of tyrosinated tubulin. Tyrosinated tubulin levels were normalized to β-tubulin levels and represented relative to the DMSO group. Mean ± SEM. ***$p < 0.001$, Mann-Whitney U test; $n = 22–37$ neurons in each group from $N = 2$ independent experiments. (D) Representative deconvolved maximum projections of STED images of detyrosinated tubulin in hippocampal neurons with and without nocodazole treatment. (E) Axonal and (F) dendritic quantification of detyrosinated tubulin. Detyrosinated tubulin levels were normalized to β-tubulin levels and represented relative to the DMSO group. **$p < 0.01$, ***$p < 0.001$, Mann-Whitney U test; $n = 28–29$ neurons from $N = 2$ independent experiments. (G) Axonal and dendritic quantification of β-tubulin in neurons immunostained for tyrosinated α-tubulin, used for quantification B and C. β-Tubulin levels are represented relative to β-tubulin levels in the DMSO group. n.s., not significant ($p > 0.05$), Mann-Whitney U test; $n = 22–37$ neurons in each group from $N = 2$ independent experiments. (H) Axonal and dendritic quantification of β-tubulin in neurons immunostained for detyrosinated α-tubulin, used for quantification in E and F. β-Tubulin levels are represented relative to β-tubulin levels in the DMSO group. n.s., not significant ($p > 0.05$), Mann-Whitney U test; $n = 28–29$ neurons in each group from $N = 2$ independent experiments.

vated peroxisomes exhibited nonprocessive motion with frequent pauses, as shown in representative kymographs (Figure 4B). Quantitative analysis of peroxisome motility in axons indicates decreased average velocities (Figure 4E) and a significantly higher number of pauses (Figure 4F) in nocodazole-treated neurons compared with the motility of peroxisomes in control experiments. Both the inhibition of processive motility and the more frequent pauses suggest a defect in dynein loading onto the plus ends of microtubules, leading to prolonged detachment of the motor from its track.

We next examined motor-induced motility in the dendrites of neurons treated with low-dose nocodazole. Consistent with our observations in axons, kinesin-induced motility was unaffected by low-dose nocodazole treatment (Figure 4G). In contrast, dynein-induced motility in dendrites was significantly reduced in nocodazole-treated neurons (Figure 4H). Unlike in axons, we did not observe a significant effect on the velocity or pausing of individual runs of dynein-driven motility in dendrites (0.67 ± 0.06 control and 0.68 ± 0.05 µm/s nocodazole-treated neurons). However, there was a significant decrease in the percentage of peroxisomes effectively transported from the dendrite back to the cell soma (Figure 4I), suggesting that dynein-driven motility was rendered less efficient by decreased microtubule dynamics.

To ensure that the observed deficits in motility were not due to a decrease in the efficiency of light-activated recruitment of dynein, we measured the increase in BICD–mCherry fluorescence following photoactivation in nocodazole-treated neurons in comparison to DMSO-treated neurons. In control neurons, photoactivation in axons induced a (4.3 ± 0.4)-fold increase in fluorescence, and in low-dose nocodazole–treated neurons we noted a (3.8 ± 0.5)-fold increase ($p > 0.05$; Student's t test). Similarly, we measured a (4.8 ± 0.5)-fold increase in fluorescence in dendrites of control neurons as compared with a (4.9 ± 1.1)-fold increase in mCherry fluorescence in dendrites of nocodazole-treated neurons ($p > 0.05$; Student's t test). Thus the decreases in peroxisome motility observed in both axons and dendrites of neurons treated with low-dose nocodazole were not due to alterations in the efficiency of dynein recruitment following photoactivation.

We also performed parallel experiments examining peroxisome motility following light-activated motor recruitment in neurons treated with low-dose paclitaxel to dampen microtubule dynamics. These experiments revealed similar defects in dynein-driven but not kinesin-driven motility induced by a loss of microtubule dynamics in both axons and dendrites (Supplemental

low-dose nocodazole (Figure 4, B and D). Although >90% of the photoactivated peroxisomes moved robustly in the retrograde direction upon recruitment of dynein in control neurons, we observed only ~60% motility following dynein recruitment in neurons treated with nocodazole (Figure 4D). The remaining ~40% of photoacti-
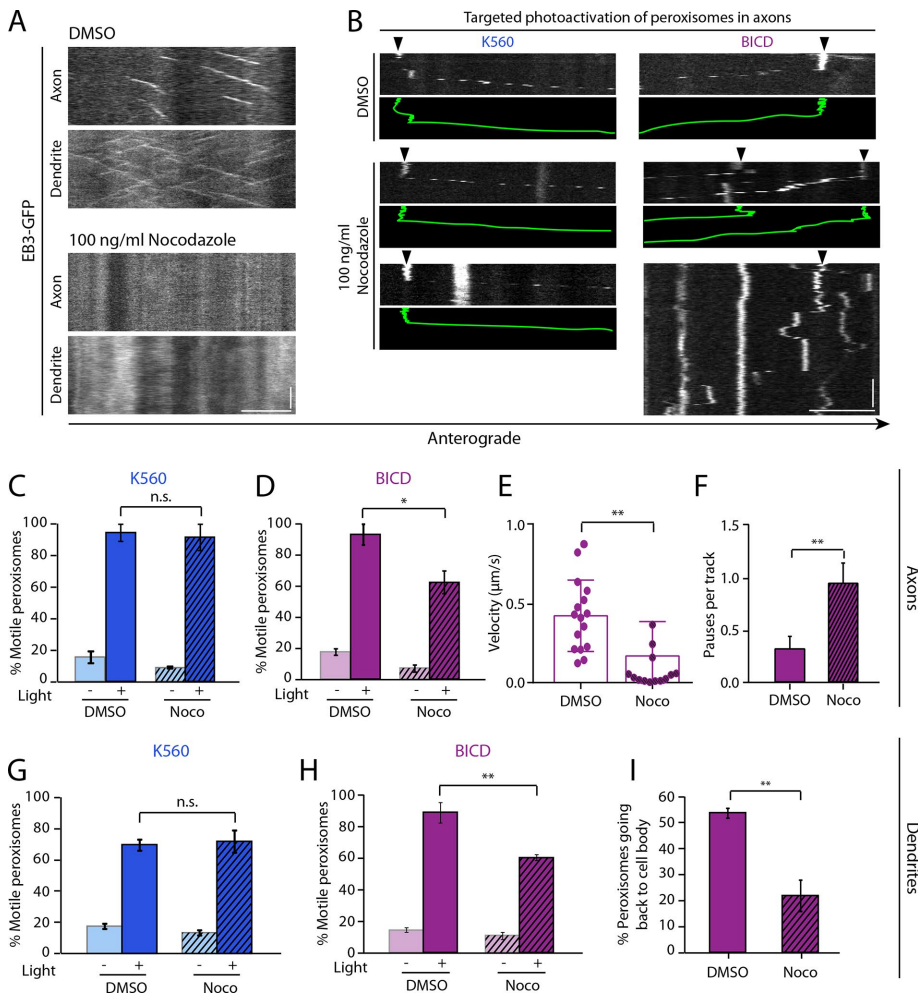
FIGURE 4: Dynein requires dynamic microtubules for efficient transport in axons and dendrites. (A) Representative kymographs of EB3 comets in axons and dendrites of hippocampal neurons treated with DMSO or 100 ng/ml nocodazole for 1.5 h at 37°C. Horizontal bar, 5 μm. Vertical bar, 30 s. (B) Representative kymographs showing movement of photoactivated peroxisomes in axons. Horizontal bar, 5 μm. Vertical bar, 1 min. (C) Quantitation of percentage of peroxisomes that are motile in axons of neurons expressing K560, treated with DMSO or nocodazole. Mean ± SEM. (D) Quantitation of percentage of peroxisomes that are motile in axons of neurons expressing BICD, mean ± SEM, (E) their average velocities, mean ± SD, and (F) number of pauses per photoactivated peroxisome, mean ± SEM. (G, H) Quantitation of percentage of peroxisomes that are motile in dendrites of neurons expressing K560 or BICD. Mean ± SEM. (I) With reduced transport in dendrites, there is a concomitant decrease in percentage of peroxisomes going back to the cell body in the case of BICD. Data from 15–20 peroxisomes, $n = 14$ neurons for axons and 25–30 peroxisomes, $n = 16$ neurons for dendrites from $N = 3$ independent experiments, n.s., not significant, $*p < 0.05$, $**p < 0.01$, Student's t test in E and H, one-way ANOVA with Tukey's post hoc test in the rest.

Figure S1). Collectively these results indicate that active microtubule dynamics lead to higher levels of tyrosinated tubulin incorporated into the lattice of both axonal and dendritic microtubules (Figure 3) and that the resulting levels of tyrosinated tubulin may promote efficient initiation of dynein-driven transport in both axonal and dendritic compartments, consistent with in vitro modeling studies (McKenney et al., 2016; Nirschl et al., 2016).

Dynein is essential for the retrograde trafficking of BDNF/TrkB signaling endosomes in dendrites

Our optogenetic data indicating that dynein efficiently navigates the dendritic cytoskeleton and that dynein-driven dendritic cargo have a clear retrograde bias suggest that this motor may play an important

role in vivo in driving retrograde trafficking of cargo from dendrite to soma. To test this prediction, we examined the contribution of dynein to the trafficking of an endogenous cargo, BDNF/TrkB-positive signaling endosomes (Liot et al., 2013). Recent work has demonstrated that similar to the axonal BDNF/TrkB complex, a major downstream function of dendritic BDNF/TrkB signaling endosomes is to modulate gene expression following active translocation to the soma (Cohen et al., 2011).

We first examined the motility of TrkB-RFP puncta in the dendrites of hippocampal neurons (Figure 5A). These puncta exhibit a retrograde bias in dendrites (Figure 5, B and C), with ~40% of total puncta moving in the retrograde direction and ~12% moving in the anterograde direction, similar to previous observations (Ghiretti et al., 2016). We treated neurons with the dynein inhibitor ciliobrevin D (20 μM) (Firestone et al., 2012; Roossien et al., 2015), which had no effect on the microtubule organization of dendrites (DMSO: 68.18 ± 2.55; ciliobrevin D: 67.09 ± 1.74; mean plus-end out ± SEM, $n = 10$ neurons from two independent experiments), but eliminated the retrograde bias in TrkB motility (Figure 5, B and C). This decreased retrograde movement in dendrites was accompanied by increases in both the anterograde and stationary pools of TrkB puncta (Figure 5C). However, we did not observe changes in the velocities of the puncta that remained motile (Figure 5D), suggesting that other motors in addition to dynein may contribute to the overall trafficking of this organelle. Next, to examine the role of microtubule dynamics in TrkB transport, we treated neurons with low-dose nocodazole and assessed the motility of TrkB-RFP. Surprisingly, unlike our observations of peroxisomes to which dynein was directly recruited (Figure 4), the dynamics of TrkB motility were unaffected by low-dose nocodazole treatment (Figure 5, B–D). Collectively these data implicate dynein in the dendritic trafficking of TrkB. However, the lack of sensitivity to nocodazole suggests

that a distinct mechanism is sufficient to induce productive engagement of TrkB-positive signaling endosomes with dendritic microtubules in the absence of dynamic microtubule plus ends enriched in tyrosinated tubulin.

Although TrkB-RFP is a marker for signaling endosomes, it is also a marker for the newly synthesized receptor found in secretory vesicles trafficking from the Golgi to the cell surface. To differentiate between these two populations, we treated neurons with BDNF-bound quantum dots (BDNF-Qdots) to more directly assess the motility of newly endocytosed ligand/receptor pairs. We observed a large colocalized population of BDNF-Qdots and TrkB-RFP moving together in dendrites (Figure 6A). This colocalization was particularly pronounced for retrogradely moving puncta. As expected, however,
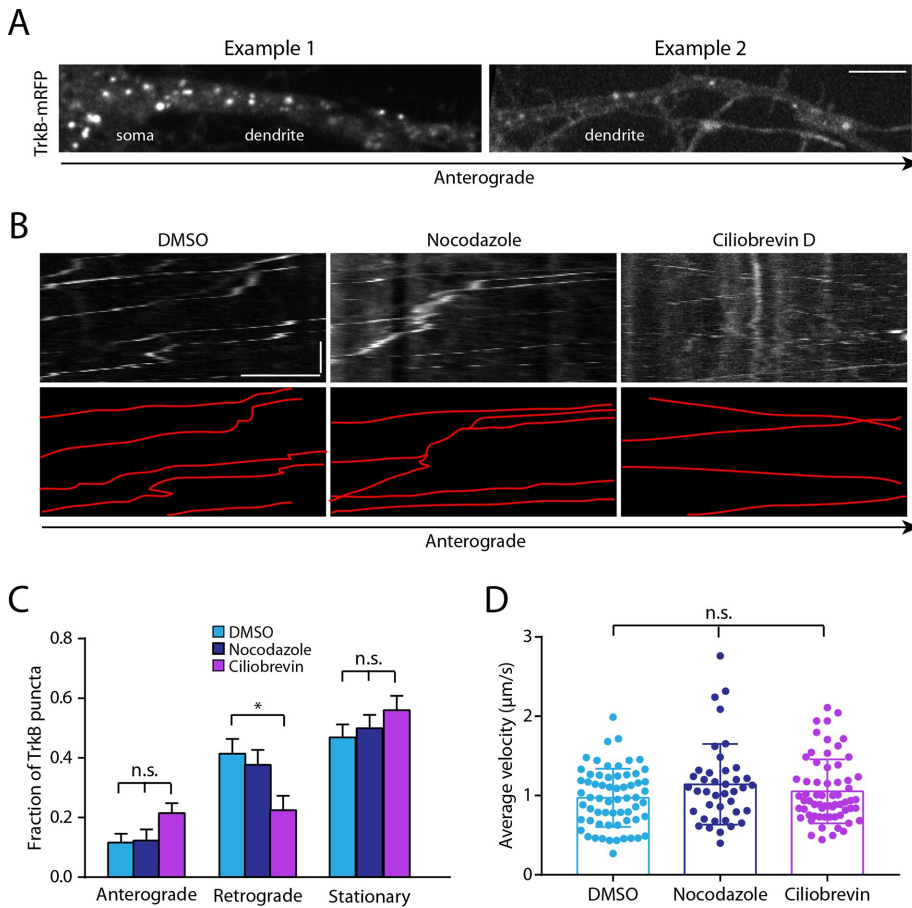
FIGURE 5: Dynein contributes to the retrograde transport of TrkB in dendrites. (A) Representative images of TrkB puncta in cell soma and dendrites of hippocampal neurons. Horizontal bar, 5 μm. (B) Representative kymographs showing the movement of TrkB-mRFP in neurons treated with DMSO or ciliobrevin D or nocodazole. (C) Fraction of TrkB puncta exhibiting anterograde or retrograde movement. Mean ± SEM. (D) Average velocities of motile TrkB puncta. Mean ± SD. Data from n = 20 neurons from N = 3 independent experiments. *p < 0.05, n.s., not significant, Student's t test.

there was also a population of TrkB-RFP+, BDNF-Qdot– puncta that likely correspond to newly synthesized TrkB receptor shuttling in dendrites (Figure 6A).

We next tested the effects of either ciliobrevin D or low-dose nocodazole treatment on the motility of internalized BDNF-Qdots, and observed very similar results to those seen with TrkB-RFP. Ciliobrevin D significantly decreased the fraction of retrogradely moving BDNF-Qdots; this inhibition of motility toward the soma was accompanied by an increase in both the anterogradely directed and stationary fractions, with no effect on average velocity (Figure 6, B–D). Nocodazole had no effect on the motility of endocytosed BDNF-Qdots, as also observed with TrkB-RFP (Figure 5, B–D). Taken together, these data suggest that dynein, which is sensitive to microtubule dynamics, is required for the proper retrograde trafficking of BDNF/TrkB complexes, but also that other motors (Ghiretti et al., 2016) may also contribute to this motility.

DISCUSSION

Using a newly developed optogenetic tool in combination with live-cell imaging, we compared the efficiency of motor-driven transport in distinct subcellular compartments of hippocampal neurons. By comparing results obtained with this optogenetic approach to the live imaging of endogenous cargoes, we could assess how an

individual motor type functions within a specific subcellular environment and also how multiple motors might contribute to the net motility of a given cargo, such as BDNF/TrkB-positive signaling endosomes. Further, our findings shed light on the different regulatory mechanisms that control cytoplasmic dynein and kinesin motility in neuronal trafficking (Figure 7).

The advantage of the optically induced recruitment assay used here is the ability to specifically target motor proteins to cargoes localized in either axons or dendrites. With this assay, we can test whether the preferential localization of endogenous motors correlates with their function—the ability of the motor to actively transport cargoes within that compartment. For kinesin-1, previous reports have shown that the constitutively active K560 construct preferentially accumulates in axon tips (Nakata and Hirokawa, 2003). In our assay, levels of soluble K560 are approximately equal in the cytoplasm of axons and dendrites, suggesting that motor availability does not differ between these compartments. In fact, we found that K560 was recruited more robustly to peroxisomes in dendrites than in axons, but the motility induced by the photoactivated recruitment of K560 to dendritic peroxisomes was not as robust as that observed in axons (~60% induced motility dendrites vs. ~90% in axons). However, those organelles that did respond following K560 recruitment exhibited motility characterized by long, bidirectional runs. Thus the kinesin-1 motor is capable of navigating the dendritic microtubule cytoskeleton when specifically recruited to dendritic organelles. This activity is likely to be physi-

ologically relevant, as full-length kinesin-1 can be steered to dendrites via GRIP1, which is found predominantly in the somatodendritic compartment (Setou et al., 2002).

In contrast to our observations of kinesin-1, we find that dynein functions as effectively in dendrites as in axons, with >90% of peroxisomes demonstrating robust motility post photoactivation in either compartment (Ballister et al., 2015, and this study). Within dendrites, dynein motility displayed a pronounced retrograde/anterograde bias (60%/40%) that correlates with the underlying organization of the microtubule cytoskeleton, with ~65% of microtubules oriented plus-end out within this region of the dendrite. Thus the directional bias in dynein motility accurately reflects the overall orientation bias of microtubule tracks within dendrites. As a consequence, dynein-induced motility caused no observable accumulation of peroxisomes at dendritic tips. Instead, ~50% of photoactivated peroxisomes eventually entered the cell soma following recruitment of BICD (Figure 2D), demonstrating that dynein effectively moves cargo from dendrites to soma.

Regulation of the dynein motor is achieved by interactions with various adaptors (King and Schroer, 2000; Huang et al., 2012; Ayloo et al., 2014; Maday et al., 2014; McKenney et al., 2014). One such ubiquitous adaptor functioning closely with dynein is the dynactin complex. We previously demonstrated that dynactin is enriched at
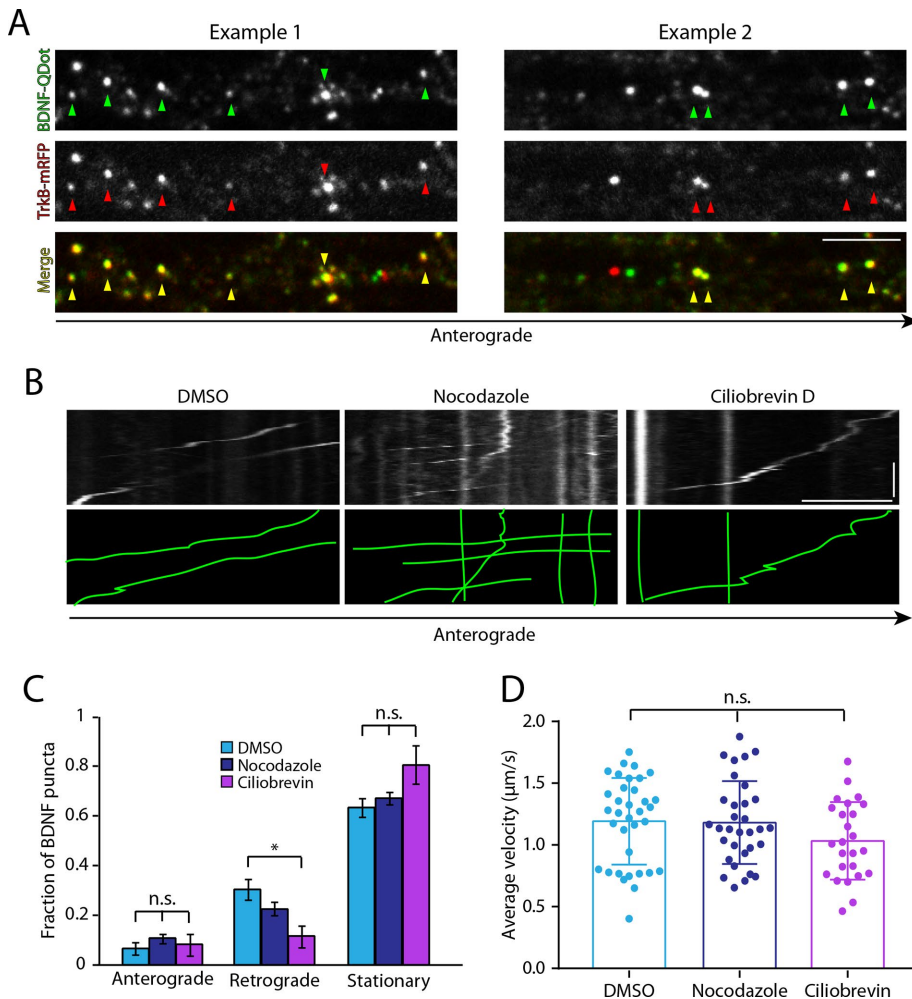
FIGURE 6: BDNF/TrkB motility in dendrites is altered by dynein inhibition. (A) Colocalization of TrkB-RFP with BDNF-Qdots in hippocampal neuron dendrites. Horizontal bar, 5 μm. (B) Representative kymographs showing the movement of BDNF-Qdots in neurons treated with DMSO or ciliobrevin D or nocodazole. (C) Fraction of BDNF-Qdots exhibiting anterograde or retrograde movement. Mean ± SEM. *$p < 0.05$, n.s., not significant, one-way ANOVA with Tukey's post hoc test. (D) Average velocities of motile BDNF-Qdots. Mean ± SD. Data from $n = 15–18$ neurons from $N = 3$ independent experiments; n.s., not significant, Student's t test.

bules following detachment of the motor from its track, although we cannot rule out the contribution of other posttranslational modifications to the microtubule cytoskeleton induced by low-dose nocodazole or low-dose paclitaxel treatment. Consistent with our hypothesis, we found that nocodazole treatment decreased the proportion of tyrosinated tubulin, which enhances the initiation of processive runs along microtubules by dynein–dynactin (McKenney et al., 2016; Nirschl et al., 2016). Although our previous observations focused on the key role of this mechanism in the initiation of axonal transport, we now speculate that the role of microtubule plus ends in facilitating motor binding may be especially important in dendrites, which have more dynamic microtubules than are observed along the midaxon (Stepanova et al., 2003; Kleele et al., 2014).

Although our observations with the optogenetic motor recruitment assay revealed several key distinctions between kinesin- and dynein-mediated trafficking within dendrites, we wanted to test the physiological relevance of our findings by analyzing the motility of an endogenous biological cargo with motility driven by a native complement of motors. We focused on BDNF/TrkB endosomes, which transit from dendrites to the soma to alter gene expression in the nucleus (Cohen et al., 2011). Analysis of the dynamics of BDNF/TrkB in dendrites revealed a key role for dynein in establishing and maintaining the retrograde bias of this cargo, as acute inhibition of dynein with ciliobrevin D significantly reduced the retrograde population of TrkB-RFP puncta while increasing the stationary and anterograde fractions. Although this observation accorded with the finding from the optogenetic assay that dy-

the distal end of axons, where highly dynamic microtubules are also enriched. Dynamic microtubules are enriched in tyrosinated tubulin and enhance the efficiency of retrograde transport initiation, as they favor the localized formation of a dynein–dynactin–CLIP-170–EB3 complex (Moughamian and Holzbaur, 2012; Moughamian et al., 2013; Nirschl et al., 2016). These observations led us to ask whether dynein motility in dendrites also requires dynamic microtubules to mediate efficient cargo motility. To test this hypothesis, we performed our photoactivation assay in neurons treated with low-dose nocodazole, which eliminates microtubule dynamics without inducing microtubule depolymerization (Vasquez et al., 1997). We observed a significant reduction in the dynein-induced motility of peroxisomes in both axons and dendrites when microtubule dynamics were inhibited. Parallel experiments performed in neurons treated with low-dose paclitaxel to dampen microtubule dynamics produced similar results. In particular, we noted a significant increase in the pausing of organelles during active runs in neurons treated with low-dose nocodazole. We propose that the decreased transport observed upon nocodazole treatment is a direct consequence of decreased reloading of dynein onto dynamic plus ends of microtu-

nein can effectively move cargo from dendrites to soma, we noted distinct findings with regard to the nocodazole sensitivity of different cargoes. Although low-dose nocodazole effectively decreased the motility of peroxisomes following optogenetic recruitment of dynein, we found that inhibition of microtubule dynamics with nocodazole had no effect on BDNF/TrkB trafficking. On the basis of this observation, and recent work demonstrating a role for KIF21B in BDNF/TrkB trafficking (Ghiretti et al., 2016), we propose that the transport of this cargo is not dependent on dynein alone, but is in fact regulated by the coordinated activity of multiple motors, including dynein, KIF21B, and potentially additional kinesin motors.

The microtubule cytoskeleton of mature neurons is organized in a way that prevents dynein-driven cargoes in the soma from entering axons but allows them to enter dendrites. A previous study using a chemical-inducible dimerization system showed that bulk recruitment of dynein to peroxisomes in steady-state assays in neurons led to a polarized redistribution of these organelles into dendrites (Kapitein et al., 2010). In our assay, we find that dynein motors specifically recruited to dendritic peroxisomes can efficiently navigate these organelles back to the cell soma. Thus our results in
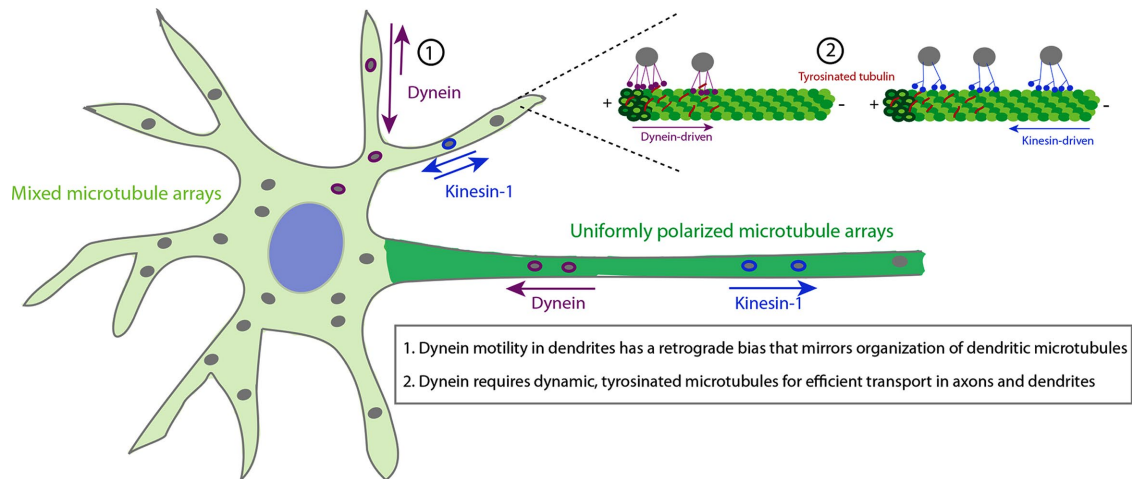
FIGURE 7: Working model for the axo-dendritic regulation of motor proteins. Microtubules are differentially organized in the axon and dendrites of mammalian neurons (shown in shades of green). Dynein (purple) motors recruited to peroxisomes using photoactivation demonstrate a retrograde bias within dendrites that reflects the overall organization of the microtubule cytoskeleton in this compartment, as 60% of microtubules are oriented with minus ends toward the soma in mammalian dendrites. In contrast, kinesin-1 (blue) motors recruited to peroxisomes show no overall directional bias in dendrites. Furthermore, efficient dynein motility requires dynamic, tyrosinated microtubules (red), whereas kinesin motility is unaffected by microtubule dynamics.

conjunction with the observations of Kapitein *et al.* (2010) demonstrate the ability of dynein to transport cargo both *into* and *out of* dendrites. Hence dynein is important not only for establishing the distribution of cargo to postsynaptic sites in dendrites (Kapitein *et al.*, 2010; van Spronsen *et al.*, 2013), but also for the efficient retrograde trafficking of cargo within the dendrite and from the dendrite back to the cell soma, a critical pathway required for cell signaling.

Polarized sorting in neurons is regulated at multiple levels; here, we focused on one aspect of this regulation, the compartment-specific interaction of motors with their microtubule tracks. Our data converge to a model wherein kinesins achieve specificity via differential interactions with microtubules in axons versus dendrites, while dynein responds to global parameters of microtubule organization, both polarity and dynamics. We find that dynein efficiently navigates the dendritic cytoskeleton, driving both anterograde and retrograde trafficking in dendrites. In vivo, the combined efforts of multiple types of motors are likely to be coordinated to regulate the motility of endogenous cargo. Together the orchestrated trafficking of organelles by these motors provides the necessary specificity to move organelles to their proper cellular locations.

MATERIALS AND METHODS
Reagents
DNA constructs for the motor recruitment assay were expressed under the CAG promoter, derived from pEM705, obtained from E. V. Makeyev (Nanyang Technological University). For peroxisome targeting, 1–42 amino acid (aa) residues of the human Pex3 gene were C-terminally fused to GFP-Halo. All the mCherry-eDHFR constructs are derived from the mCherry-eDHFR plasmid previously described in Ballister *et al.* (2014). BICD–mCherry–eDHFR constitutes residues 1–572 of mouse BICD2 (referred to herein as BICD according to Kapitein *et al.* [2010]) and K560–mCherry–eDHFR includes residues 1–560 of human kinesin-1 heavy chain (Ballister *et al.*, 2015; Kapitein *et al.*, 2010). TrkB-mRFP was provided by M. Chao (New York University). Antibodies used in immunofluorescence assays were rat anti-

tyrosinated α-tubulin, clone YL1/2 (MAB1864; 2 μg/ml) and rabbit anti-detyrosinated α-tubulin (AB3201; 2 μg/ml) from EMD Millipore, and mouse anti–β-tubulin (T5201; 8 μg/ml) from Sigma-Aldrich; goat anti-rat Alexa Fluor 555 (A-21434; 8 μg/ml), goat anti-rabbit Alexa Fluor 555 (A-21428; 8 μg/ml), and goat anti-mouse Oregon Green 488 (O-6380; 8 μg/ml) from ThermoFisher Scientific.

Neuronal cell culture, transfections, and drug treatment
Sprague Dawley rat hippocampal neurons were dissected from embryos at days 18–20 as described (Wilcox *et al.*, 1994) and obtained in suspension from the Neuron Culture Service Center at the University of Pennsylvania. Cells (100,000/ml) were plated on 35 mm glass-bottomed dishes coated with 0.5 mg/ml poly-L-lysine. Neurons were grown in 2 ml maintenance media (neurobasal medium supplemented with 2% B-27, 33 mM glucose, 2 mM GlutaMax, 100 U/ml penicillin, and 100 μg/ml streptomycin) at 37°C in a 5% CO_2 incubator. Every 3–4 d, 25% of the media was replaced with fresh maintenance media supplemented with 1 μM AraC.

Imaging was done at 8–10 DIV (days in vitro) with DNA plasmids transfected 12–18 h before imaging. PEX3-GFP-Halo was cotransfected with motor protein construct (either K560-mCherry-eDHFR or BICD-mCherry-eDHFR) using Lipofectamine 2000 reagent (ThermoFisher Scientific).

Neurons were imaged in low-fluorescence nutrient media (Hibernate E, Brain Bits) supplemented with 2% B27 and 1% GlutaMax. In all experiments, neurons were incubated with 10 μM of the caged dimerizer cTMP-Halo (Ballister *et al.*, 2014) for 30 min. The excess ligand was washed away with imaging media before imaging. For low-dose nocodazole and paclitaxel experiments, neurons were treated with 100 ng/ml nocodazole (Sigma) or 200 nM paclitaxel (Cytoskeleton) for 1.5 h, as noted, at 37°C in a 5% CO_2 incubator. Ciliobrevin D (EMD Millipore) was used at 20 μM for 1.5 h; we find that in the presence of B27 and GlutaMax, the drug has a less profound effect on axonal transport than that reported by Sainath and Gallo (2015) but more selectively inhibits retrograde rather than anterograde axonal transport. BDNF-biotin (Alomone Labs) was

conjugated to Qdot 655 Streptavidin (ThermoFisher Scientific) and BDNF-Qdots were added to hippocampal neurons as previously described (Ghiretti et al., 2016).

Image acquisition and photoactivation
Data were acquired on a spinning-disk confocal UltraView VOX (Perkin Elmer) with a 405 nm Ultraview Photokinesis (Perkin Elmer) unit on an inverted Nikon Ti microscope with apochromat 100×1.49 NA oil-immersion objective and a C9100-50 EMCCD camera (Hamamatsu) controlled by Volocity software (Perkin Elmer). Only neurons expressing both of the cotransfected GFP and mCherry markers were imaged. Axons and dendrites were identified based on morphologic criteria as outlined (Kaech and Banker, 2006). Localized photoactivation along axons was performed as described (Ballister et al., 2015). At 8–10 DIV, dendrite lengths in our cultures were ~50–200 μm. Peroxisomes localized approximately to the middle one-third of dendrites were selected for photoactivation. Two-color images (GFP and mCherry) were acquired for 20 s at 2 s per frame before photoactivation and for 5 min at 2 s per frame postphotoactivation. EB3-GFP and TrkB-mRFP imaging was recorded at 1 frame/s; BDNF-Qdot imaging was recorded at 2 frames/s.

Motility analysis
Photoactivated organelles were classified as motile if they moved greater than a 5 μm distance in our 5 min imaging window. For axonal data, all velocities reported are average velocities. In dendrites, the motion was considered bidirectional if the organelle moved greater than 5 μm in both the anterograde and retrograde directions at least once during motion. All run length and velocity measurements were made from kymographs drawn using the Kymograph plug-in in Fiji (Schindelin et al., 2012).

For dendrite data, run length and velocities were obtained for every constant velocity segment in a given trajectory of an organelle. Owing to the depth of the dendrites, only organelles that could clearly be tracked for the entire length of the movie were considered for run length and velocity analysis. Each kymograph was generated in both the GFP and mCherry channels to correlate organelle movement with that of the recruited motor. For the quantitation of pauses per track in Figure 4F, motion with a velocity of less than 0.05 μm/s was considered a pause. TrkB and BDNF puncta in dendrites were scored as anterograde, retrograde, or stationary using a 10 μm distance cutoff. All dendrites in a field of view for a given neuron were analyzed and all velocities reported for TrkB and BDNF are average velocities.

Fluorescence measurements for recruitment
All intensity measurements for the recruitment analysis were recorded using Fiji. A region of interest (ROI) was drawn enclosing the organelle. The mean intensity of mCherry fluorescence in this ROI was measured 1 frame before photoactivation and 1 frame before the organelle started to move. In both cases, the cytoplasmic background was subtracted. Postphotoactivation intensity was then divided by prephotoactivation intensity to obtain fold change indicating recruitment of the motor protein or motor adaptor.

Immunofluorescence
Rat primary hippocampal neurons on 25 mm round glass coverslips were fixed at 9–10 DIV in phosphate-buffered saline (PBS) containing 4% paraformaldehyde and 4% sucrose for 5 min. Coverslips were washed three times in PBS and blocked/permeabilized with PBS containing 5% normal goat serum, 1% bovine serum albumin (BSA), and 0.1% Triton X-100. Primary antibodies

(either anti-tyrosinated α-tubulin + anti–β-tubulin or anti-detyrosinated α-tubulin + anti–β-tubulin) were diluted in antibody dilution (Abdil) solution (1% BSA and 0.1% Triton X-100 in PBS) and incubated with the coverslips overnight at 4°C. After removing the primary antibodies and three washes with PBS, the coverslips were incubated with fluorophore-conjugated secondary antibodies diluted in Abdil for 45 min at room temperature. Following six washes with PBS, the coverslips were mounted on glass slides in ProLong Gold Antifade Mountant (ThermoFisher Scientific) and sealed with nail polish.

STED microscopy and measurement of microtubule tyrosination
Imaging of immunostained neurons was performed on the spinning-disk confocal system described above using an apochromat 60× or 100×1.49 NA oil-immersion objective and on a Leica DMI 6000 microscope equipped with 592 and 660 nm STED depletion lasers using a 100×1.4 NA oil-immersion objective. STED z-stacks images were acquired using the Leica Application Suite X and deconvolved using Huygens Professional software (Scientific Volume Imaging) with the Classical Maximum Likelihood Estimation algorithm. Acquisition and deconvolution parameters were kept constant for intensity comparisons between treatments.

Measurement of dendritic α-tubulin tyrosination or detyrosination intensity levels in each neuron was performed on maximum projections and were normalized against the respective β-tubulin signal. The relative α-tubulin tyrosination or detyrosination levels per neuron in the DMSO and nocodazole groups were then calculated against the average intensity value of the respective DMSO-treated group.

Statistical methods
All statistics were performed in GraphPad Prism. A Student's t test or a Mann-Whitney U test was used when comparing two data sets, as indicated, while a one-way analysis of variance (ANOVA) with Tukey's post hoc test was used with multiple data sets.

REFERENCES
Arpag G, Shastry S, Hancock WO, Tuzel E (2014). Transport by populations of fast and slow kinesins uncovers novel family-dependent motor characteristics important for in vivo function. Biophys J 107, 1896–1904.

Ayloo S, Lazarus JE, Dodda A, Tokito M, Ostap EM, Holzbaur EL (2014). Dynactin functions as both a dynamic tether and brake during dynein-driven motility. Nat Commun 5, 4807.

Baas PW, Deitch JS, Black MM, Banker GA (1988). Polarity orientation of microtubules in hippocampal neurons: uniformity in the axon and non-uniformity in the dendrite. Proc Natl Acad Sci USA 85, 8335–8339.

Ballister ER, Aonbangkhen C, Mayo AM, Lampson MA, Chenoweth DM (2014). Localized light-induced protein dimerization in living cells using a photocaged dimerizer. Nat Commun 5, 5475.

Ballister ER, Ayloo S, Chenoweth DM, Lampson MA, Holzbaur EL (2015). Optogenetic control of organelle transport using a photocaged chemical inducer of dimerization. Curr Biol 25, R407–R408.

Bentley M, Decker H, Luisi J, Banker G (2015). A novel assay reveals preferential binding between Rabs, kinesins, and specific endosomal subpopulations. J Cell Biol 208, 273–281.

Cohen MS, Bas Orth C, Kim HJ, Jeon NL, Jaffrey SR (2011). Neurotrophin-mediated dendrite-to-nucleus signaling revealed by microfluidic

compartmentalization of dendrites. Proc Natl Acad Sci USA 108, 11246–11251.

Farkhondeh A, Niwa S, Takei Y, Hirokawa N (2015). Characterizing KIF16B in neurons reveals a novel intramolecular "stalk inhibition" mechanism that regulates its capacity to potentiate the selective somatodendritic localization of early endosomes. J Neurosci 35, 5067–5086.

Firestone AJ, Weinger JS, Maldonado M, Barlan K, Langston LD, O'Donnell M, Gelfand VI, Kapoor TM, Chen JK (2012). Small-molecule inhibitors of the AAA+ ATPase motor cytoplasmic dynein. Nature 484, 125–129.

Ghiretti AE, Thies E, Tokito MK, Lin T, Ostap EM, Kneussel M, Holzbaur EL (2016). Activity-dependent regulation of distinct transport and cytoskeletal remodeling functions of the dendritic kinesin KIF21B. Neuron 92, 857–872.

Huang CF, Banker G (2012). The translocation of the kinesins that mediate neuronal organelle transport. Traffic 13, 549–564.

Huang J, Roberts AJ, Leschziner AE, Reck-Peterson SL (2012). Lis1 acts as a "clutch" between the ATPase and microtubule-binding domains of the dynein motor. Cell 150, 975–986.

Jacobson C, Schnapp B, Banker GA (2006). A change in the selective trans-location of the kinesin-1 motor domain marks the initial specification of the axon. Neuron 49, 797–804.

Jenkins B, Decker H, Bentley M, Luisi J, Banker G (2012). A novel split kinesin assay identifies motor proteins that interact with distinct vesicle populations. J Cell Biol 198, 749–761.

Kaech S, Banker G (2006). Culturing hippocampal neurons. Nat Protoc 1, 2406–2415.

Kapitein LC, Schlager MA, Kuijpers M, Wulf PS, van Spronsen M, MacKintosh FC, Hoogenraad CC (2010). Mixed microtubules steer dynein-driven cargo transport into dendrites. Curr Biol 20, 290–299.

King SJ, Schroer TA (2000). Dynactin increases the processivity of the cyto-plasmic dynein motor. Nat Cell Biol 2, 20–24.

Kleele T, Marinkovic P, Williams PR, Stern S, Weigand EE, Engerer P, Naumann R, Hartmann J, Karl RM, Bradke F, et al. (2014). An assay to image neuro-nal microtubule dynamics in mice. Nat Commun 5, 4827.

Liot G, Zala D, Pla P, Mottet G, Piel M, Saudou F (2013). Mutant Hunting-tin alters retrograde transport of TrkB receptors in striatal dendrites. J Neurosci 33, 6298–6309.

Lloyd TE, Machamer J, O'Hara K, Kim JH, Collins SE, Wong MY, Sahin B, Imlach W, Yang Y, Levitan ES, et al. (2012). The p150(Glued) CAP-Gly domain regulates initiation of retrograde transport at synaptic termini. Neuron 74, 344–360.

Maday S, Twelvetrees AE, Moughamian AJ, Holzbaur EL (2014). Axonal transport: cargo-specific mechanisms of motility and regulation. Neuron 84, 292–309.

McKenney RJ, Huynh W, Tanenbaum ME, Bhabha G, Vale RD (2014). Activa-tion of cytoplasmic dynein motility by dynactin-cargo adapter com-plexes. Science 345, 337–341.

McKenney RJ, Huynh W, Vale RD, Sirajuddin M (2016). Tyrosination of α-tubulin controls the initiation of processive dynein-dynactin motility. EMBO J 35, 1175–1185.

Moughamian AJ, Holzbaur EL (2012). Dynactin is required for transport initiation from the distal axon. Neuron 74, 331–343.

Moughamian AJ, Osborn GE, Lazarus JE, Maday S, Holzbaur EL (2013). Ordered recruitment of dynactin to the microtubule plus-end is required for efficient initiation of retrograde axonal transport. J Neurosci 33, 13190–13203.

Muhia M, Thies E, Labonte D, Ghiretti AE, Gromova KV, Xompero F, Lappe-Siefke C, Hermans-Borgmeyer I, Kuhl D, Schweizer M, et al. (2016). The kinesin KIF21B regulates microtubule dynamics and is essential for neuronal morphology, synapse function, and learning and memory. Cell Rep 15, 968–977.

Nakata T, Hirokawa N (2003). Microtubules provide directional cues for polarized axonal transport through interaction with kinesin motor head. J Cell Biol 162, 1045–1055.

Nirschl JJ, Magiera MM, Lazarus JE, Janke C, Holzbaur EL (2016). α-Tubulin tyrosination and CLIP-170 phosphorylation regulate the initiation of dynein-driven transport in neurons. Cell Rep 14, 2637–2652.

Prevo B, Mangeol P, Oswald F, Scholey JM, Peterman EJ (2015). Functional differentiation of cooperating kinesin-2 motors orchestrates cargo import and transport in C. elegans cilia. Nat Cell Biol 17, 1536–1545.

Roossien DH, Miller KE, Gallo G (2015). Ciliobrevins as tools for studying dynein motor function. Front Cell Neurosci 9, 252.

Ruane PT, Gumy LF, Bola B, Anderson B, Wozniak MJ, Hoogenraad CC, Allan VJ (2016). Tumour suppressor Adenomatous Polyposis Coli (APC) locali-sation is regulated by both kinesin-1 and kinesin-2. Sci Rep 6, 27456.

Sainath R, Gallo G (2015). The dynein inhibitor ciliobrevin D inhibits the bidirectional transport of organelles along sensory axons and impairs NGF-mediated regulation of growth cones and axon branches. Dev Neurobiol 75, 757–777.

Schindelin J, Arganda-Carreras I, Frise E, Kaynig V, Longair M, Pietzsch T, Preibisch S, Rueden C, Saalfeld S, Schmid B, et al. (2012). Fiji: an open-source platform for biological-image analysis. Nat Methods 9, 676–682.

Setou M, Seog DH, Tanaka Y, Kanai Y, Takei Y, Kawagishi M, Hirokawa N (2002). Glutamate-receptor-interacting protein GRIP1 directly steers kinesin to dendrites. Nature 417, 83–87.

Song AH, Wang D, Chen G, Li Y, Luo J, Duan S, Poo MM (2009). A selective filter for cytoplasmic transport at the axon initial segment. Cell 136, 1148–1160.

Splinter D, Razafsky DS, Schlager MA, Serra-Marques A, Grigoriev I, Demmers J, Keijzer N, Jiang K, Poser I, Hyman AA, et al. (2012). BICD2, dynactin, and LIS1 cooperate in regulating dynein recruitment to cellular structures. Mol Biol Cell 23, 4226–4241.

Stepanova T, Slemmer J, Hoogenraad CC, Lansbergen G, Dortland B, De Zeeuw CI, Grosveld F, van Cappellen G, Akhmanova A, Galjart N (2003). Visualization of microtubule growth in cultured neurons via the use of EB3-GFP (end-binding protein 3-green fluorescent protein). J Neurosci 23, 2655–2664.

van Spronsen M, Mikhaylova M, Lipka J, Schlager MA, van den Heuvel DJ, Kuijpers M, Wulf PS, Keijzer N, Demmers J, Kapitein LC, et al. (2013). TRAK/Milton motor-adaptor proteins steer mitochondrial trafficking to axons and dendrites. Neuron 77, 485–502.

Vasquez RJ, Howell B, Yvon AM, Wadsworth P, Cassimeris L (1997). Nano-molar concentrations of nocodazole alter microtubule dynamic instabil-ity in vivo and in vitro. Mol Biol Cell 8, 973–985.

Wilcox KS, Buchhalter J, Dichter MA (1994). Properties of inhibitory and excitatory synapses between hippocampal neurons in very low density cultures. Synapse 18, 128–151.

Yogev S, Cooper R, Fetter R, Horowitz M, Shen K (2016). Microtubule orga-nization determines axonal transport dynamics. Neuron 92, 449–460.